Passively stable 0.7-octave microcombs in thin-film lithium niobate microresonators

Zexing Zhao (赵泽兴)[1], Chenyu Wang (王晨宇)[1], Jingyuan Qiu (邱静远)[2], Zhilin Ye (叶志霖)[2], Zhijun Yin (尹志军)[2], Zhenlin Wang (王振林)[1], Kunpeng Jia (贾琨鹏)[1*], Xiao-Hui Tian (田晓慧)[1**], Zhenda Xie (谢臻达)[1***], and Shi-Ning Zhu (祝世宁)[1]

[1] National Laboratory of Solid State Microstructures, School of Electronic Science and Engineering, School of Physics, College of Engineering and Applied Sciences, and Collaborative Innovation Center of Advanced Microstructures, Nanjing University, Nanjing 210093, China

[2] Nanzhi Institute of Advanced Optoelectronic Integration Technology Co., Ltd., Nanjing 210093, China

*Corresponding author: jiakunpeng@nju.edu.cn
**Corresponding author: tianxiaohui@nju.edu.cn
***Corresponding author: xiezhenda@nju.edu.cn

The optical frequency comb based on microresonators (microcombs) is an integrated coherent light source and has the potential to promise a high-precision frequency standard; self-reference and a long-term stable microcomb are the keys to this realization. Here, we demonstrated a 0.7-octave spectrum Kerr comb via dispersion engineering in a thin-film lithium niobate microresonator, and the single-soliton state can be accessed passively with long-term stability over 3 h. With such a robust broadband coherent comb source using thin-film lithium niobate, a fully stabilized microcomb can be expected for massive practical applications.

1. Introduction

As a highly coherent light source, the optical frequency comb generated on the microresonator (so-called microcomb) has many applications, thanks to its high integrity, low power consumption, and low phase noise[1,2]. Especially, octave-spanning microcombs via dispersion engineering can realize a chip-scale 2f-3f or f-2f[3,4] self-referencing scheme. This makes it a potential new frequency standard because of its high precision[5,6]. In practice, the stability of the soliton comb source is the basis of subsequent signal processing. However, achieving a long-term stable soliton comb can be challenging due to thermal effects or center frequency jitter induced by the pump. This often requires a complex feedback system, which hinders the minimization of the device[7–10].

In recent years, thin-film lithium niobate (LN) photonic devices have been greatly developed and studied because of their broadband low-loss optical transparent window, excellent quadratic nonlinear effect, and high electro-optic efficiency[11–20]. In particular, the optical intensity-dependent photorefractive effect of LN[21,22] is just opposite to the thermo-optic nonlinear effect, so it enables a new mechanism for effectively generating soliton optical frequency combs based on an LN microresonator with self-starting property[23,24]. Furthermore, such a feature

is potentially beneficial for long-term passive stability of the soliton comb, which is of significance for practical applications.

In this Letter, we report soliton microcombs generated in z-cut LN-on-insulator (LNOI) thin-film microring resonators (MRRs), and different states of soliton microcomb generation are observed. Moreover, the balance of photorefractive and thermo-optical effects of LN facilitates the generation of passively stable single-soliton for more than 3 h without feedback control. Finally, a wideband Kerr comb is generated in the MRR with a smaller size based on dispersion engineering. We demonstrate the potential of high-performance LN microresonators as integrated, highly robust, and broadband coherent laser sources on a chip.

2. Designs and Fabrications

The high-Q LNOI resonators are fabricated by a standard e-beam lithography process. We initially use the electron beam to pattern the device on photoresist, and then the waveguide is fabricated by an Ar-ion milling process. Figures 1(a) and 1(b) show an optical image of the MRR device and the cross section of the waveguide. The LN thin film (0.62 µm thickness) is partially etched down by 0.32 µm, and the sidewall angle (θ) is estimated
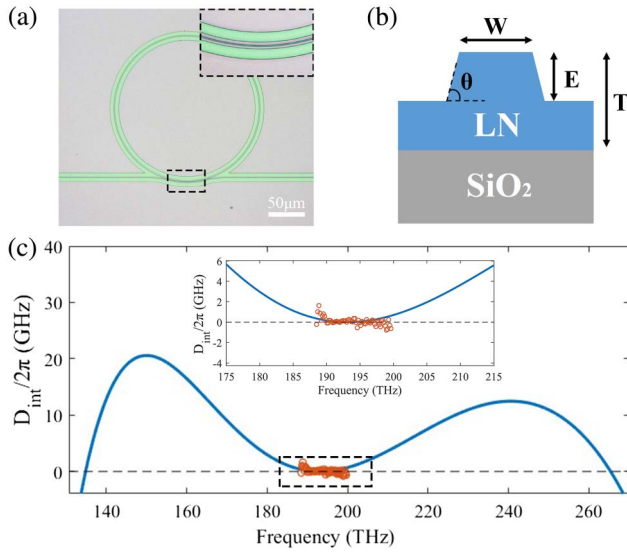
Fig. 1. (a) Optical image of the LNOI microring resonator; inset, zoom-in of the coupling region; (b) cross-sectional schematic of the LN waveguide, with W (width) of 1.6 µm, E (etch depth) of 0.32 µm, and T (thickness) of 0.62 µm; (c) simulated LN waveguide integrated dispersion $D_{int}/(2\pi)$ (blue); inset, local zoom-in within the black dashed box with the experimentally extracted data points (orange circles).
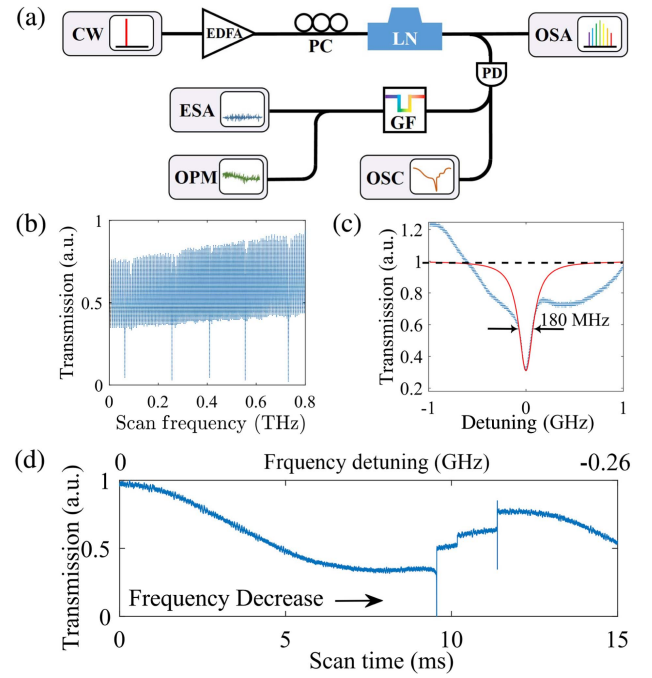

Fig. 2. (a) Schematic of experimental testing setups, including CW (continuous wave) source, EDFA (erbium-doped fiber amplifier), PC (polarization controller), PD (photodetector), OSC (oscilloscope), OSA (optical spectrum analyzer), ESA (electrical spectrum analyzer), GF (grating filter), and OPM (optical power meter); (b) MRR transmission spectrum in a slightly undercoupled state; (c) laser cavity detuning of the pump resonance mode (blue dot) with fitting Lorentz curve (red); (d) resonator transmission at a high-power pump when the laser frequency decreased.

to be about 70°. The entire device is air-clad. We prepare the LN MRRs with different radii of 100 and 60 µm, corresponding to the free spectral ranges (FSRs) of 200 and 333 GHz, respectively. We obtain anomalous dispersion in a wide spectral band by optimizing the geometry of the waveguide[25]. We used the single-layer inversed taper as the end-coupling structure with an estimated coupling efficiency of 13%. We simulate the D_{int} curve [Fig. 1(c), left, blue] of the MRR with a radius of 100 µm, and the zero D_{int} matching points are around 135 and 270 THz, identified as the position of the dispersive wave (DW). The inset is a zoom-in view of the black dashed box. We measure the resonant frequencies in transmission curve of the microresonator by scanning the laser frequency[23,24] and extract the waveguide dispersion at 1550 nm band by fitting the D_{int} curves.

3. Experiments and Discussions

The schematic of the experimental setup is shown in Fig. 2(a). The continuous-wave laser is amplified by an erbium-doped fiber amplifier and coupled into the cavity through lens fiber as the pump light. We first measure the MRR transmission spectrum in the telecom band. The pump polarization is adjusted to match the TE cavity mode by the polarization controller (PC). The output optical signal is detected by a photodetector and followed by an oscilloscope to record the cavity mode transmission. The result is shown in Fig. 2(b). Figure 2(c) is the zoom-in view of the selected cavity mode, and the Lorentzian fitting (red curve) indicates an extracted Q_L of over one million. As the power increases, we observe the appearance of soliton steps

when the scanning pump light frequency decreases, as shown in Fig. 2(d). The output microcomb spectrum is measured by an optical spectrum analyzer [Fig. 2(a)]. Furthermore, we use the grating filter to suppress the pump mode. The extracted comb power is characterized by an electrical spectrum analyzer and optical power meter.

Different soliton comb states can be achieved by manually changing the pump frequency with the spectra shown in Figs. 3(a)–3(h). Figure 3(d) shows a single-soliton comb with a repetition rate of 200 GHz, and the spectral envelope is fitted by the sech^2 function (red). However, we notice that the measured comb spectra feature no dispersive wave, which is perhaps caused by insufficient on-chip power ($\sim$260 mW). In addition, we also observe the two-soliton-state combs [Figs. 3(e) and 3(f)]. Moreover, the low-frequency RF signal of generated combs in each state is measured to confirm the low-noise soliton state[24].

Figures 3(i) and 3(j) show the change of comb power during the generation of a long-term single-soliton comb. We first manually tune the off-resonance pumped laser [Fig. 3(i), I region] frequency increase continuously until it excites the four-wave mixing process [Fig. 3(i), II region]. After the appearance of the soliton state, we decrease the pumped laser frequency and keep the frequency constant once reaching the single-soliton state [Fig. 3(i), III region].
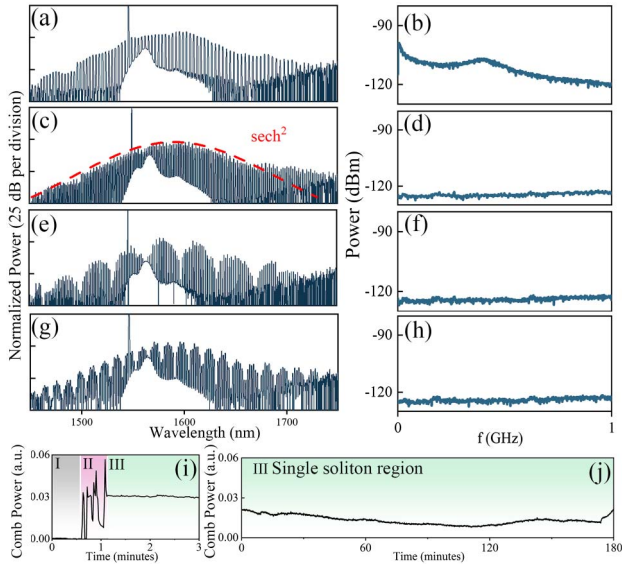
Fig. 3. Characterization of frequency combs generated on LN microresonator (radius 100 μm). The frequency comb spectra in different states are characterized, including (a) chaos comb, (c) single-soliton comb, and (e), (g) two-soliton combs with different relative angles between solitons. The mode-locked single-soliton comb was featured with a sech^2 fitting curve [(c), red dotted line]. Furthermore, the intensity noise of the all frequency combs was characterized and shown in the right panel corresponding to each graph [(b), (d), (f), (h)]. The stable generation of the single soliton for the long term is realized by photorefractive and thermo-optical effects [(i) and (j)].

The long-term stability of the microcomb is a key parameter for practical applications. Figure 3(j) shows the optical power of a single-soliton state as a function of time. The single-soliton state can be preserved for over 3 h, showing excellent passive stability. In the process of microcomb generation in the LN microresonator, the thermal effect detunes the cavity mode toward the red region, while the photorefractive effect of LN detunes it toward the blue region[21,22]. Therefore, the photorefractive effect can compensate for the thermal effect of the microresonator and facilitate a stable soliton microcomb state[22,23].

The comb span is limited by the on-chip power in the 200 GHz MRRs, and we use 333 GHz MRRs for the broadband comb generation. With similar on-chip power, the circulating pump power is higher due to the higher finesse at the same Q. Figure 4(a) is the simulated D_{int} curve in this case of geometric parameters; the designed DWs are located at 1315 nm and 2120 nm. At the pump power of ∼220 mW, we observe the broadband microcomb generation [Fig. 4(b)]. The DWs generated by the Cherenkov radiation are located at 1250 and 2010 nm, respectively, and the range of the comb line is from 1230 to 2100 nm (∼0.7-octave). We find that the measured positions of DWs deviated from the simulation and a blueshift occurred. Because LN is highly Raman-active, the existence of Raman scattering will eventually produce a Raman–Kerr optical frequency comb in soliton, forming a dynamic process[24]. It changes the condition for zero D_{int} point and causes the DWs
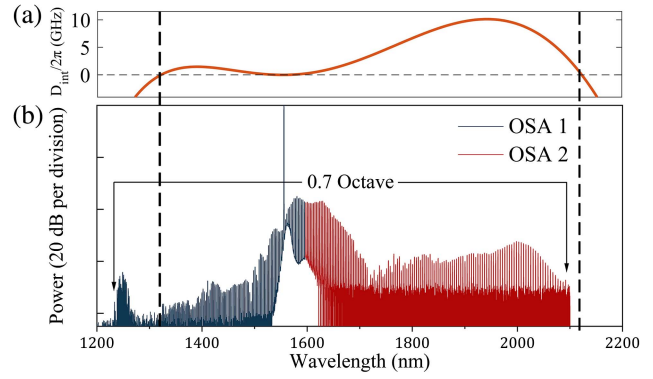

Fig. 4. Spectral characteristics of the LN microresonator (radius 60 μm) as well as simulation; the black dashed line marks the position of the dispersive wave in experimental results. (a) Simulated D_{int} curves; (b) normalized optical spectrum of the wideband Kerr comb.

of the spectrum to be blueshifted. The broadband Kerr optical frequency comb via dispersion engineering can be further exploited such as 2f-3f reference technology research. For the 200 GHz MRRs, it is expected that the double-layer taper structure could provide sufficient on-chip power to realize the generation of an octave soliton comb, which can be used for an integrated all-optical self-reference locking scheme.

4. Conclusions

In conclusion, we have demonstrated soliton microcombs generated on the LN platform based on the photorefractive effect. We fabricate a high Q z-cut LN MRR by using a standard e-beam lithography process. In the experiment, a simple single-layer taper is used for end coupling, with a measured coupling efficiency of 13%. We test the stability of the single-soliton state in the pure free-running setup, and the results show that the single soliton state can be passively stabilized for over 3 h. Furthermore, the 0.7-octave spanning Kerr comb is observed with high stability, which can be expected to be used in 2f-3f self-referencing technology. In addition, the rich optical properties of LNOI make it possible for fully integrated self-referenced optical frequency comb realization. For example, the excellent electro-optic coefficient of LN can be used to generate a microcomb with high-speed modulation capability, providing extra freedoms for dynamic control and active feedback for integrated microcomb sources. Such properties can be further applied to large-scale optical communication, microwave photonic technology, and other fields.

Acknowledgements

References

1. T. J. Kippenberg, A. L. Gaeta, M. Lipson, *et al.*, "Dissipative Kerr solitons in optical microresonators," Science **361**, eaan8083 (2018).
2. P. Trocha, M. Karpov, D. Ganin, *et al.*, "Ultrafast optical ranging using microresonator soliton frequency combs," Science **359**, 887 (2018).
3. V. Brasch, E. Lucas, J. D. Jost, *et al.*, "Self-referenced photonic chip soliton Kerr frequency comb," Light Sci. Appl. **6**, e16202 (2017).
4. Q. Li, T. C. Briles, D. A. Westly, *et al.*, "Stably accessing octave-spanning microresonator frequency combs in the soliton regime," Optica **4**, 193 (2017).
5. S. A. Diddams, K. Vahala, and T. Udem, "Optical frequency combs: coherently uniting the electromagnetic spectrum," Science **369**, eaay3676 (2020).
6. Z. L. Newman, V. Maurice, T. Drake, *et al.*, "Architecture for the photonic integration of an optical atomic clock," Optica **6**, 680 (2019).
7. V. Brasch, M. Geiselmann, M. H. P. Pfeiffer, *et al.*, "Bringing short-lived dissipative Kerr soliton states in microresonators into a steady state," Opt. Express **24**, 29312 (2016).
8. N. G. Pavlov, S. Koptyaev, G. V. Lihachev, *et al.*, "Narrow-linewidth lasing and soliton Kerr microcombs with ordinary laser diodes," Nat. Photon. **12**, 694 (2018).
9. A. S. Raja, A. S. Voloshin, H. Guo, *et al.*, "Electrically pumped photonic integrated soliton microcomb," Nat. Commun. **10**, 680 (2019).
10. C. Joshi, J. K. Jang, K. Luke, *et al.*, "Thermally controlled comb generation and soliton modelocking in microresonators," Opt. Lett. **41**, 2565 (2016).
11. J. Lu, J. B. Surya, X. Liu, *et al.*, "Periodically poled thin-film lithium niobate microring resonators with a second-harmonic generation efficiency of 250,000%/W," Optica **6**, 1455 (2019).
12. A. Roy, R. Nehra, S. Jahani, *et al.*, "Temporal walk-off induced dissipative quadratic solitons," Nat. Photonics **16**, 162 (2022).
13. C. Wang, M. Zhang, M. Yu, *et al.*, "Monolithic lithium niobate photonic circuits for Kerr frequency comb generation and modulation," Nat. Commun. **10**, 978 (2019).
14. C. Wang, M. Zhang, X. Chen, *et al.*, "Integrated lithium niobate electro-optic modulators operating at CMOS-compatible voltages," Nature **562**, 101 (2018).
15. M. He, M. Xu, Y. Ren, *et al.*, "High-performance hybrid silicon and lithium niobate Mach–Zehnder modulators for 100 Gbit s^{-1} and beyond," Nat. Photon. **13**, 359 (2019).
16. M. Xu, M. He, Y. Zhu, *et al.*, "Flat optical frequency comb generator based on integrated lithium niobate modulators," J. Light. Technol. **40**, 339 (2022).
17. R. Gao, N. Yao, J. Guan, *et al.*, "Lithium niobate microring with ultra-high Q factor above 10^8," Chin. Opt. Lett. **20**, 011902 (2022).
18. Q. Luo, C. Yang, Z. Hao, *et al.*, "On-chip erbium-doped lithium niobate waveguide amplifiers," Chin. Opt. Lett. **19**, 060008 (2021).
19. M. G. Vazimali and S. Fathpour, "Applications of thin-film lithium niobate in nonlinear integrated photonics," Adv. Photonics **4**, 034001 (2022).
20. G. Chen, N. Li, J. D. Ng, *et al.*, "Advances in lithium niobate photonics: development status and perspectives," Adv. Photonics **4**, 034003 (2022).
21. X. Sun, H. Liang, R. Luo, *et al.*, "Nonlinear optical oscillation dynamics in high-Q lithium niobate microresonators," Opt. Express **25**, 13504 (2017).
22. Y. Xu, M. Shen, J. Lu, *et al.*, "Mitigating photorefractive effect in thin-film lithium niobate microring resonators," Opt. Express **29**, 5497 (2022).
23. Y. He, Q.-F. Yang, J. Ling, *et al.*, "Self-starting bi-chromatic LiNbO$_3$ soliton microcomb," Optica **6**, 1138 (2019).
24. Z. Gong, X. Liu, Y. Xu, *et al.*, "Near-octave lithium niobate soliton microcomb," Optica **7**, 1275 (2020).
25. V. Brasch, M. Geiselmann, T. Herr, *et al.*, "Photonic chip–based optical frequency comb using soliton Cherenkov radiation," Science **351**, 357 (2016).